Lattice dynamics and thermodynamic properties of $NaAlH_4$: Density-functional calculations using a linear response theory

A. Peles and M. Y. Chou
School of Physics, Georgia Institute of Technology, Atlanta, Georgia 30332-0430, USA
(Received 7 November 2005; revised manuscript received 21 February 2006; published 4 May 2006)

We present a first-principles investigation of the lattice dynamics and thermodynamical properties of a complex hydride $NaAlH_4$, a promising material for hydrogen storage. The calculations are performed within the density-functional-theory framework and using a linear response theory. Calculations of the phonon spectrum, Born effective charges Z^*, and dielectric constants in high and low frequency limits are reported. The mode characters of the zone-center phonons, including the LO-TO splitting, are identified and compared to the experiment. The quasiharmonic approach is used to study thermal expansion as well as the mean square displacement of each atom as a function of temperature. A connection is established between the latter and the melting point. The inclusion of the zero-point motion leads to an expanded lattice compared to the static lattice, while the low frequency oscillations are found to play an important role in the melting and decomposition of $NaAlH_4$.

DOI: 10.1103/PhysRevB.73.184302 PACS number(s): 63.20.−e, 71.15.Mb, 65.40.−b, 77.22.−d

I. INTRODUCTION

In the past decade the need for clean, renewable, and efficient energy sources has become increasingly important; hydrogen is the most promising energy carrier for the future.[1–3] The fuel-cell technology powered by hydrogen exists already. However, an efficient way of storing hydrogen, especially for mobile applications, remains a challenge. A recent discovery of the reversible hydrogenation/dehydrogenation processes in $NaAlH_4$ under moderate conditions and upon doping with a small amount of Ti has reintroduced complex hydrides of light metals as viable hydrogen storage materials.[4] Hydrogen release from $NaAlH_4$ accompanies a decomposition process which proceeds through a series of chemical reactions:[4]

$$NaAlH_4 \rightarrow \tfrac{1}{3}Na_3AlH_6 + \tfrac{2}{3}Al + H_2\uparrow$$

$$Na_3AlH_6 \rightarrow 3NaH + Al + \tfrac{3}{2}H_2\uparrow$$

$$NaH \rightarrow Na + \tfrac{1}{2}H_2\uparrow .$$

$NaAlH_4$ has 5.6 wt % hydrogen available excluding hydrogen release in the NaH decomposition which occurs at too high of a temperature for practical applications.

A number of experimental and theoretical research efforts have been devoted to studying $NaAlH_4$.[5] The way additives (Ti, Zr, Fe, etc.) accelerate reactions and affect the reversibility of these reactions has not been understood up to date. Elucidating physical properties and processes in the undoped $NaAlH_4$ is an important step in that direction. The decomposition process of both pure and doped (Ti, Zr) alanates have been studied experimentally by means of *in situ* x-ray diffraction suggesting a high mobility of metal or metal-hydrogen species in pure $NaAlH_4$.[6] Valuable insight into the decomposition process and hydrogen evolution can be gained through lattice dynamics studies. The lattice dynamics of $NaAlH_4$ has been investigated experimentally using Raman spectroscopy,[7–9] infrared spectroscopy,[9,10] neutron incoherent scattering,[10] and inelastic incoherent neutron scattering.[11] Thermodynamic functions including the free energy and specific heat of $NaAlH_4$ have been measured in the temperature range from 15 to 300 K.[12] However, no such measurements have been reported in the literature for a temperature range from 300 K and up to the melting point of the compound. The experimental data on the dielectric properties are also lacking to our knowledge. A number of theoretical studies of the electronic structure of the $NaAlH_4$ have been reported.[5,13–16] The recent first-principles linear response calculations of phonon frequencies accompanying the polarized Raman spectroscopy measurements found that the observed dramatic softening of the low frequency Raman modes near the melting point is essentially due to an anharmonic mechanism beyond the lattice expansion.[8] The same study hypothesized that breaking up of the AlH_4 anions is the rate-limiting step for the hydrogen release in the first chemical reaction.[8] The decomposition reactions of $NaAlH_4$ have also been investigated based on the thermodynamic functions where the phonon dispersion and phonon density of states have been calculated by a direct force-constant method using the projector augmented wave (PAW) method.[17] In addition, the phonon density of states calculation that reproduced well the measured neutron inelastic scattering spectrum suggested sharp two-phonon features.[11]

In this paper we present a comprehensive study of lattice dynamics and thermodynamical properties of $NaAlH_4$ using the first-principles approach based on density functional theory and linear response theory. In particular, the importance of low-energy vibrations, dominated by the motion of the metal (Na) and metal-hydrogen complex (AlH_4), for the melting process of undoped sodium alanate is identified. The large anharmonicity associated with these modes together with calculated mean square displacements suggest that the periodicity of lattice is broken by large and inelastic displacements of Na^+ and AlH_4^- species. The thermal energy available to the system up to the melting point is not sufficient to significantly excite hydrogen vibrations within the

AlH_4 complex and to modify the Al-H bonding strength. Thus, thermally activated release of hydrogen is hindered in pure $NaAlH_4$ below the melting point as it was observed by experiment.[3,6] The appropriate description of exchange-correlation effects in electron-electron interactions is explored for $NaAlH_4$ by using both the local density approximation (LDA) and generalized gradient approximation (GGA). We have found that structural and vibrational properties depend significantly on the choice of exchange-correlation functionals (LDA versus GGA). To illustrate, inclusion of the density gradient in the exchange-correlation approximation (GGA) predicts a 30% smaller bulk modulus than those predicted by LDA. Thermal expansion and vibrational frequencies are also affected by the choice of the exchange-correlation functional.

Details of the computational methodology are summarized in Sec. II. Section III has the results of our study organized in five parts. Part A presents a detailed study of lattice geometry in both LDA and GGA approximations. Dielectric and vibrational properties at the center of Brillouin zone are presented in part B. Part C discusses the phonon dispersion and phonon density of states. The effect of zero-point vibrations on the structural properties of $NaAlH_4$ is presented in part D. Part E presents thermodynamical properties and treats anharmonicity within a quasiharmonic approximation. The conclusions are presented in Sec. IV.

II. CALCULATIONAL METHODS

The present calculations were performed within the density functional theory (DFT)[18,19] framework using norm-conserving pseudopotentials of the Troullier-Martins[20] type. The electron exchange-correlation energy was evaluated using both the local density approximation (LDA),[21] and the generalized gradient approximation (GGA),[22] and a comparison between the two functionals is made. The plane-wave cutoff energy of 25 hartrees and a $4\times4\times4$ k-point grid for summations over the Brillouin zone were found sufficient. The pseudopotentials were generated from the following valence states: Al $(3s^23p^13d^0)$ with cutoff radii of 1.79 a.u. (s), 1.97 a.u. (p) and 2.12 a.u. (d); Na $(3s^13p^0)$ with cutoff radii of 2.70 a.u. (s) and 2.70 a.u. (p); and H $(1s^1)$with a cutoff radius of 1.28 a.u. The partial core correction method[23] was applied in the generation of Na pseudopotentials to account for the nonlinearity of the exchange-correlation functional. The dynamical matrix elements were calculated on the $4\times4\times4$ grid of k points using a linear-response approach. The linear responses to nuclear displacements and electric fields were calculated within density functional perturbation theory (DFPT) as implemented in the ABINIT code.[24]

III. RESULTS AND DISCUSSIONS

A. Lattice structure and symmetry considerations

The crystal symmetry of $NaAlH_4$ is body-centered tetragonal with a centro-symmetric space group $I4_1/a$[25–27] and a corresponding 4/m point group. A primitive unit cell consists of two formula units. Na and Al atoms occupy sites of tetragonal point symmetry $(\bar{4})$, while hydrogen atoms reside on general position sites with a lowest site symmetry (1). Al atoms are surrounded by four nearest neighbor H atoms and form almost perfect tetrahedra, as shown in Fig. 1. The individual tetrahedral complexes $(AlH_4)^-$ are negatively charged while Na^+ are positively charged and ionocally bonded. The binding within the AlH_4^- complex is covalent in nature but with a large ionicity. The crystal structure is defined by two lattice constants plus three internal structural parameters specifying the position coordinates x, y, and z of hydrogen atoms not fixed by the space group. The optimal static geometries within LDA and GGA are determined by energy and force minimization starting from the experimental structure. The residual force and stress in the equilibrium geometries are of the order of 10^{-5} hartree/a.u. and 10^{-3} GPa, respectively. The equilibrium lattice constants a and c and internal parameters calculated using LDA and GGA exchange-correlation approximations are given in Table I together with experimental values, calculated bulk moduli under the condition of isotropic stress, and the pressure derivative of the bulk modulus at equilibrium volume. The bulk modulus and its pressure derivative are obtained using the Murnaghan equation of state.

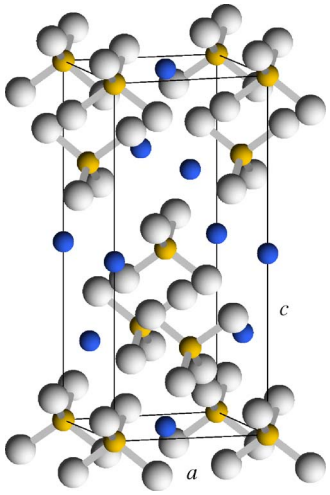

FIG. 1. (Color online) Crystal structure of tetragonal $NaAlH_4$. Na atoms are represented by blue (dark) spheres. Tetragonal AlH_4 complex is shown with respective Al-H bonds. The central aluminum atoms are shown by small gold (dark gray) spheres, while hydrogen atoms are represented by large white (light grey) spheres.

Comparing with the experimental results,[25–27] well-known features of both LDA and GGA approximations are apparent. LDA overbinding results in lattice parameters a and c that are 1.8% and 3.8% smaller than experimental values, respectively, while the inclusion of a density gradient in GGA relaxes the binding and improves the agreement with experiment, giving the parameter a 0.2% larger and parameter c 0.7% smaller than experimental ones. Here, the zero-point vibrations are not included. The vibrational properties will be discussed in later sections. By including the zero-point vibrations, lattice constants within both LDA and GGA will increase and they are listed in Table I. LDA lattice parameters a and c remain lower than experimental values by −0.4 and −2.3%, respectively, while GGA parameters are overestimated by 1.4% in a and 1.3% in c. The large difference in

TABLE I. Calculated lattice parameters, internal parameters, and bulk moduli at $T=0$ with and without the zero-point motion for tetragonal $NaAlH_4$.

Lattice constants (Å)	a	c	
Without zero-point motion			
LDA (This work)	4.89	10.72	
GGA (This work)	4.99	11.07	
LDA (Ref. 33)	4.83	10.56	
GGA (Ref. 33)	4.99	11.07	
GGA (Ref. 17)	4.979	11.103	
With zero-point motion			
LDA (This work)	4.96	10.90	
GGA (This work)	5.05	11.28	
GGA (Ref. 17)	5.044	11.330	
Expt. (8 K)[a]	4.9802	11.1482	
Expt. (10 K)[b]	4.993	11.196	
Internal parameters	x	y	z
LDA	0.2356	0.3996	0.5408
GGA	0.2355	0.3921	0.5440
Expt. (8 K)[a]	0.2371	0.3867	0.5454
Bulk modulus (GPa)	$B_0=\left(\frac{d^2F}{dV^2}\right)_{P=0}$	$B'=\left(\frac{dB}{dP}\right)_{P=0}$	
Without zero-point motion			
LDA	27.4	4.9	
GGA	17.7	4.7	
With zero-point motion			
LDA	25.4	4.9	
GGA	14.7	4.7	

[a]Reference 27.
[b]Reference 9.

the calculated bulk modulus within LDA and GGA approximations further illustrates the importance of the way the exchange and correlation effects are treated in density functional methods in general. The GGA static-lattice bulk modulus is ~35% lower when compared to the LDA static-lattice bulk modulus. Inclusion of the zero-point vibration softens the bulk modulus in both cases, while the difference increases by a few percent. To our knowledge the experimental value for the bulk modulus of $NaAlH_4$ has not been reported in the literature. The fact that LDA and GGA predict significantly different bulk moduli suggests that the calculated dynamical properties including vibrational frequencies and thermal expansion will be different using different exchange-correlation functionals.

In order to assess if our theoretical structure is the true equilibrium and to avoid instabilities when performing phonon calculations, we disturbed hydrogen positons of our optimal structure by displacing atoms by approximately 1% of the lattice constant, losing all symmetry except the inversion symmetry, and then performing the structural relaxation. The relaxation led to hydrogen position parameters differing within 10^{-4} from the previous results and recovered all symmetry operations of the $I4_1/a$ space group showing that our structure is indeed stable.

B. Dielectric and vibrational properties at Γ

There are twelve atoms in the primitive unit cell of $NaAlH_4$ hence 36 normal modes of vibrations. This gives rise to rather complex vibrational properties due to the occurrence of the LO-TO splitting induced by the long-range Coulomb interactions in this ionic material $[Na^{+1}(AlH_4)^{-1}]$. In order to account for such splitting at the Γ point ($\mathbf{q}=0$), knowledge of the Born effective charge and high frequency dielectric tensors is essential as such knowledge allows the nonanalytical long-range part of the dynamical matrix to be calculated in the long wavelength limit.[28] The dependence of the nonanalytical part of the dynamical matrix $\mathbf{C}^{NA}(\mathbf{q}\rightarrow\mathbf{0})$ on the Born effective charge tensor $\mathbf{Z}^*$ and dielectric tensor $\boldsymbol{\epsilon}^{\infty}$ is given as

$$C^{NA}_{k\alpha,k'\beta}(\mathbf{q}\rightarrow\mathbf{0})=\frac{4\pi}{\Omega_0}\frac{\left(\sum_{\gamma} q_{\gamma} Z^*_{k,\gamma\alpha}\right)\left(\sum_{\gamma'} q_{\gamma'} Z^*_{k',\gamma'\beta}\right)}{\sum_{\mu\nu} q_{\mu}\epsilon^{\infty}_{\mu\nu} q_{\nu}}, \quad (1)$$

where Ω_0 denotes primitive unit-cell volume, k and k′ label atoms, and the Greek symbols label directions.

The Born effective charge tensor and dielectric tensor in the low and high frequency limits were calculated within a linear response theory and their principal values are listed in Table II. In the reference frame with the z axis along the crystallographic axis c, $\mathbf{Z}^*$'s of Na and Al atoms are diagonal and anisotropic with $Z^*_{xx}=Z^*_{yy}\neq Z^*_{zz}$ as expected for sites with tetragonal symmetry. H atoms, situated at the low symmetry site, have nondiagonal and anisotropic Z^*. The hydrogen Z^* has one principal axis within a few degrees along the Al-H bond and the corresponding principal values close to the nominal charge of H (−1) within a complex. The Born effective charge components of Al are smaller than its nominal charge (+3) while Na has a slightly larger Z^* than its nominal charge (+1). The calculated dielectric tensors are anisotropic in accordance with symmetry and likely overestimated due to the error in the band gap value inherent in density functional approaches. There is no experimental value for the dielectric tensor of $NaAlH_4$ available at present. In order to make a prediction, we use the previously calculated theoretical quasiparticle band gap correction to the GGA band gap[16] and implement a shift of conduction band eigenvalues (scissor shift), yielding corrected dielectric constant components of 2.34 and 2.43 along the a and c axes, respectively. The components of $\boldsymbol{\epsilon}^0$ are much larger than those of $\boldsymbol{\epsilon}^{\infty}$ as a consequence of the significant contribution to the low-frequency dielectric permitivity tensor due to ionic displacements. The calculated GGA Born effective charges agree well with the recent GGA-PAW calculation.[17] The LDA Born effective charges and dielectric tensor are also in a good agreement with reported LDA values.[8] These previously published results are also listed in Table II. In addition we observe a decrease in the dielectric constants when the scissor shift is applied to the conduction bands. The scissor correction has been found crucial in reproducing the experimental values for the dielectric constants for materials like Si and it would be interesting to experimentally test how these effects are important for alanates.

TABLE II. Calculated principal values of Born effective charge tensors Z^* for Na, Al, and H, dielectric constant tensors ϵ^∞ and ϵ^0 in high and low frequency limits, respectively, within both LDA and the GGA approaches.

Principal values	$Z^*_{x'x'}$	$Z^*_{y'y'}$	$Z^*_{z'z'}$
LDA (This work)			
Na	1.12	1.12	1.00
Al	1.66	1.66	2.09
H	-0.59	-0.68	-0.89
GGA (This work)			
Na	1.20	1.20	1.09
Al	1.67	1.67	2.04
H	−0.61	−0.67	−0.93
LDA (Ref. 8)			
Na	1.16	1.16	1.04
Al	1.67	1.67	2.12
H	−0.61	−0.68	−0.90
GGA (Ref. 17)			
Na	1.20	1.20	1.09
Al	1.64	1.64	2.01
H	−0.60	−0.69	−0.91
ϵ^∞	ϵ^∞_{xx}	ϵ^∞_{yy}	ϵ^∞_{zz}
LDA (This work)	3.42	3.42	3.62
GGA (This work)	3.12	3.12	3.28
GGA (This work)[a]	2.34	2.34	2.43
LDA (Ref. 8)	3.5	3.5	3.7
ϵ^0	ϵ^0_{xx}	ϵ^0_{yy}	ϵ^0_{zz}
LDA (This work)	9.50	9.50	8.06
GGA (This work)	10.10	10.10	8.64
LDA (Ref. 8)	10.1	10.1	9.2

[a]With scissor correction (see text).

The group symmetry decomposition into irreducible representations of the 4/m point group at the Γ point yields a sum of E_u+A_u for three acoustic modes and $3A_g+5B_g+5E_g+4A_u+3B_u+4E_u$ for the 33 optical modes. The centrosymmetric groups have infrared and Raman active modes that are mutually exclusive. All modes symmetric with respect to inversion, namely, the g modes, are Raman active. Among the u modes, which are antisymmetric with respect to inversion, the A_u and E_u modes may induce a nonzero dipole moment both parallel with and perpendicular to the phonon propagation direction. They are infrared active and exhibit a LO-TO splitting.

The vibrational spectrum of the individual tetrahydroaluminate complex (AlH_4^-) has been measured experimentally in both the solvated and the solid states of $LiAlH_4$ and $NaAlH_4$ salts,[29] as well as in an inert gas matrix isolation of the complex.[30] The AlH_4^- species was identified as having identical Al-H bond lengths and forming nearly perfect tetrahedra. Consequently, the assignment of measured frequencies was done assuming the tetrahedral symmetry, namely, the T_d point group. A symmetry decomposition of the T_d point group allows for four distinct vibrations of the tetrahedral AlH_4^- complex in addition to rigid translations and rotations. These are symmetric stretch $\nu_1(A_1)$, symmetric bend $\nu_2(E)$, asymmetric stretch $\nu_3(F_2)$, and asymmetric bend $\nu_4(F_2)$. The vibrational modes of a tetrahedral molecule are identified and illustrated by Herzberg[31] and we follow the same notation here. The normal mode of A_1 symmetry is nondegenerate, while the modes having E and F_2 symmetry are doubly and triply degenerate, respectively. All modes are Raman active and only the F_2 modes are infrared active.

Within the $NaAlH_4$ solid, the T_d symmetry of isolated complex changes into the symmetry of tetragonal site $(\bar{4})$. Furthermore, the two complexes within each primitive unit cell are related by inversion, with an inversion center midway between two Al atoms. Thus the T_d degeneracy is being lifted and the modes split. The splitting and connection between the modes of isolated and inversion-related complexes are as follows: $2A_1 \rightarrow A_g+B_u$; $2E \rightarrow A_g+B_g+A_u+B_u$; $2F_2 \rightarrow B_g+E_g+A_u+E_u$. The extent of the T_d mode splitting in the crystal environment gives an indication of the coupling strength of the AlH_4^- complex within a crystal. Table III lists both the LDA and GGA normal-mode frequencies at the theoretical equilibrium volumes of the static lattice and at the experimental volume. The assignments, according to the bulk 4/m and the appropriate T_d point group, are listed as well as experimentally measured frequencies. The LO-TO splitting was determined from the projection of the Born effective charges along the displacement directions of the eigenmodes. Four groups of modes can be identified. The low frequency group of modes up to $\sim$200 cm^{-1} represents the translational motions of Na^+ and AlH_4^- relative to each other. The next group higher in frequency between $\sim$360–560 cm^{-1} represents hindered rotations of AlH_4^- complex. The next group with frequencies between $\sim$550–860 cm^{-1} corresponds to hydrogen bending and the highest frequency group of modes above 1600 cm^{-1} consists of hydrogen stretches, symmetric and antisymmetric. The lowest and highest groups are well separated by distinct frequency gaps from the other two groups of modes with intermediate frequencies. However, the gap between the vibrational and hydrogen bending modes is diminishing. These low frequency modes were measured in the early '70s[10] and also in a recent study.[7] The phonon frequencies estimated at the experimental volume are in reasonable agreement with experiment for both LDA and GGA. The hydrogen vibration frequencies at the experimental volume obtained with GGA are larger than those within LDA, especially ν_1, ν_2, and ν_4. The ν_3 frequency is within a few cm^{-1} between LDA and GGA predicted frequencies, while low frequency translatory and librational modes have larger values with LDA than with GGA. The measured as well as the calculated Raman frequencies[8] at the Γ point agree reasonably well with our results. The good agreement of Γ point frequencies is also found with the GGA-PAW study[17] including the predicted LO-TO splitting of infrared modes. We point out that experimentally observed infrared frequencies are those of isolated AlH_4 complex only and no experimental values of the LO-TO splitting have been reported yet.

TABLE III. The phonon frequencies in cm^{-1} for optical normal modes at the Γ point calculated at equilibrium lattice constants. The values in parentheses are calculated at the experimental lattice parameters. Raman modes calculated in Ref. 8 are also included.

	LDA		GGA		Experiment
Mode symmetry	ω_{TO}	ω_{LO}	ω_{TO}	ω_{LO}	
Infrared active:					
A_u (tran.)	180 (153)	181 (161)	138 (135)	153 (150)	
E_u (tran.)	195 (169)	227 (209)	155 (154)	201 (201)	
E_u (rot.)	372 (364)	440 (405)	364 (362)	401 (397)	
A_u [$\nu_2(E)$]	525 (551)	703 (710)	557 (561)	738 (740)	688[c],752[c]
E_u [$\nu_4(F_2)$]	727 (696)	846 (819)	693 (697)	839 (838)	
A_u [$\nu_4(F_2)$]	890 (848)	944 (899)	866 (864)	915 (913)	901[c]
A_u [$\nu_3(F_2)$]	1661 (1623)	1731 (1694)	1614 (1614)	1695 (1694)	1678[c]
E_u [$\nu_3(F_2)$]	1692 (1655)	1757 (1720)	1648 (1647)	1724 (1723)	
Raman active:	This work	Ref. 8	This work	Ref. 8	
E_g (tran.)	141 (125)	135	116 (115)	116	107[a],117[d]
B_g (tran.)	130 (119)	128	120 (118)	101	116[a],125[d]
B_g (tran.)	227 (190)	220	183 (178)	182	174[a],178[b],184[d]
E_g (tran.)	212 (194)	210	189 (189)	191	184[d]
A_g (tors.)	514 (464)	512	461 (458)	458	419[a],432.5[d]
E_g (tors.)	616 (562)	614	566 (561)	560	511[a],494[b],524[d]
A_g [$\nu_2(E)$]	776 (751)	759	744 (746)	748	765[a],764[b],767[c],771[d]
B_g [$\nu_2(E)$]	797 (776)	786	792 (791)	797	812[a],799[b],824[c],817[d]
E_g [$\nu_4(F_2)$]	840 (796)	822	813 (811)	817	847[a],861[b],848[d]
B_g [$\nu_4(F_2)$]	860 (826)	844	847 (846)	850	
E_g [$\nu_3(F_2)$]	1699 (1657)	1681	1655 (1653)	1649	1680[a],1686[c],1684[d]
B_g [$\nu_3(F_2)$]	1724 (1686)	1706	1681 (1681)	1673	1782[d]
A_g [$\nu_1(A_1)$]	1748 (1716)	1729	1731 (1730)	1726	1769[a],1790[b],1763[c],1774[d]
Inactive:					
B_u (rot.)	496 (478)		506 (503)		
B_u [$\nu_2(E)$]	881 (829)		840 (834)		
B_u [$\nu_1(A_1)$]	1759 (1722)		1738 (1737)		

[a]Reference 7.
[b]Reference 10.
[c]Reference 29.
[d]Reference 8.

C. Phonon dispersion and density of states

Phonon dispersion curves along high symmetry lines in the Brillouin zone are plotted in Fig. 2. As the Γ point is approached from different directions ($\mathbf{q}\rightarrow 0$) the infrared E_u and A_u phonon mode branches approach different limiting values at Γ ($\mathbf{q}=0$), as expected. The four separate bands can be identified in Fig. 2. To find out which atomic species participate in these vibrations, we calculate a partial phonon density of states as follows:

$$g_n(\omega) = \frac{1}{3N}\sum_{\mathbf{k},j} |\mathbf{e}_n(\mathbf{k},j)|^2 \delta[\omega - \omega(\mathbf{k},j)], \qquad (2)$$

where n denotes the particular atom (H, Al or Na), $\mathbf{k}$ is the wave vector, j is the index of phonon branches in the spectrum, N is total number of atoms in an unit cell, and $\mathbf{e}_n(\mathbf{k},j)$ is the normalized phonon polarization vector such that $\Sigma_n|\mathbf{e}_n(\mathbf{k},j)|^2=1$. A $46\times46\times46$ grid of k points was employed. The total and projected phonon density of states are plotted as a function of frequencies in Fig. 3 where four bands can clearly be seen. The lowest frequency band with frequencies in the range of 0–200 cm^{-1} is dominated by the motion of Na and Al atoms. The higher frequency bands are dominated by H vibrations, with Al participation to much lesser extent. Here we presented the GGA calculations in order to compare with similar calculations using the GGA-PAW approach.[17] Our calculated dispersion curves are similar to those reported in Ref. 17. Both calculations show the dependence of energy on the wave vector direction when approaching the Γ point, resulting in LO-TO splitting. The agreement in the total and partial densities of states in the two calculations is also good.

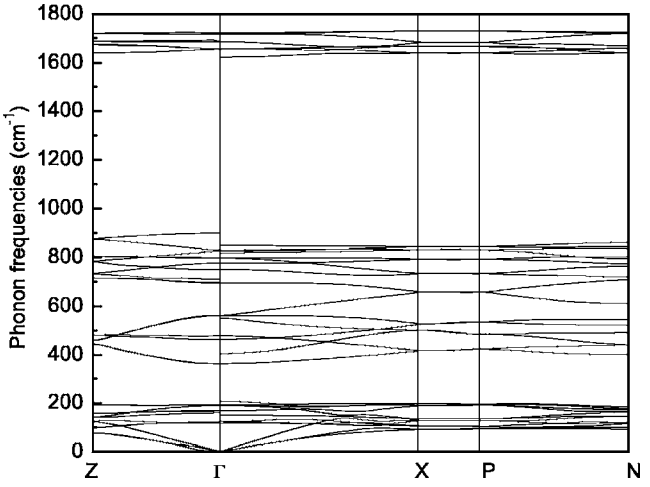

FIG. 2. Calculated phonon dispersion curves along symmetry lines for $NaAlH_4$ using GGA at the theoretical volume.

D. The effect of zero-point motion on structural properties of $NaAlH_4$

The high vibrational frequencies of light hydrogen atoms are expected to result in a significant zero-point energy which is known to modify the zero-temperature ground-state structural properties. It is therefore pertinent to ascertain the zero-point energies and their effect on the static lattice structure. The zero-point energy at a given volume is calculated as follows:

$$F_{zp}(V) = \frac{1}{2}\sum_{\mathbf{k},n} \hbar\,\omega_n(\mathbf{k},V) = 3N\int_0^{\omega_{max}} \frac{\hbar\,\omega}{2} g(\omega,V)d\omega, \quad (3)$$

where N is a number of atoms in the unit cell, n denotes normal modes, and $g(\omega,V)$ is phonon density of states at volume V normalized in such a way that $\int_0^{\omega_{max}} g(\omega,V)d\omega=1$. The c/a ratio is fixed in this calculation. Within the two exchange-correlation approximations, the zero-point energies at theoretical geometries are 0.0609 and 0.05867 hartree/cell for LDA and GGA, respectively. This zero-point energy contribution increases the free lattice energy. Its volume dependence can be seen as introducing a negative pressure that ultimately increases the equilibrium volume of static lattice. The expected change in volume can be estimated from

$$\frac{\Delta V}{V_0} = -\frac{\Delta P}{B_0}, \quad (4)$$

where ΔV is the difference between the equilibrium volume determined with and without the zero-point motion at zero temperature, $\Delta P = -\frac{\partial F_{zp}(V)}{\partial V} = -\frac{\hbar}{2}\Sigma_{\mathbf{k},n}\frac{\partial \omega_n(\mathbf{k},V)}{\partial V}$ is a zero-point pressure, and V_0 and B_0 are the volume and isothermal bulk modulus of a static lattice. A similar increase in the lattice volume is predicted within two approximations, namely 4.4% and 4.3% for LDA and GGA, respectively. Figure 4 illustrates the energy dependence on volume for the static lattice $E(V)$ and also the vibrating lattice $E(V)+F_{zp}(V)$ at zero temperature when the c/a ratio is kept constant. There is an increase of 4.5% in equilibrium volume when quantum mechanical oscillations at zero temperature are included. This is an unusually large change for a typical solid. Although the c/a ratio is fixed here, the predicted volume expansion due to zero-point motion agrees well with the results obtained by taking into account independent variations of a and c. The details will be described in the following section.

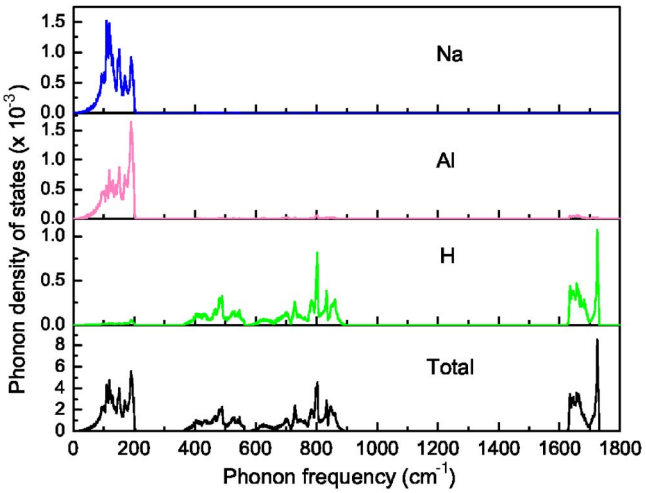

FIG. 3. (Color online) Total and projected phonon density of states calculated using GGA at the theoretical volume.

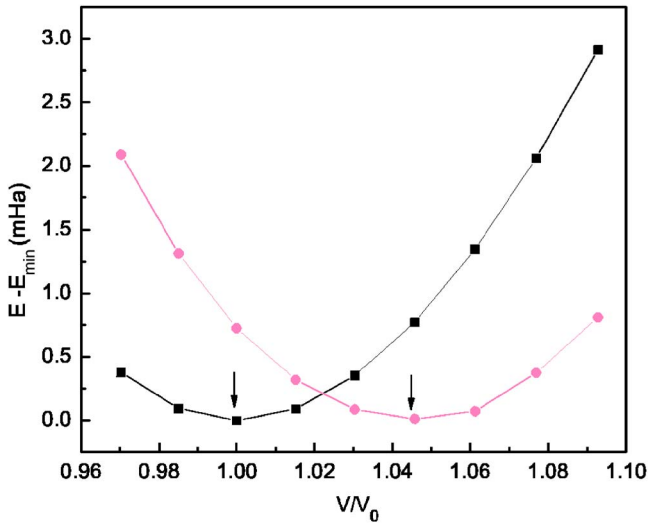

FIG. 4. (Color online) Volume dependence of the LDA total energy per unit cell at zero temperature for both the static lattice energy $E(V)$ (squares) and vibrating lattice energy $E(V)+F_{zp}(V)$ (circles). The energy of each curve is shifted by its minimum E_{min} for clarity. The equilibrium static volume increases about 4.5% when the zero-point motion energy is included.

E. Thermodynamical properties

The specific heat at constant volume is calculated using a standard expression for noninteracting harmonic oscillators corresponding to the normal modes of crystal as follows:

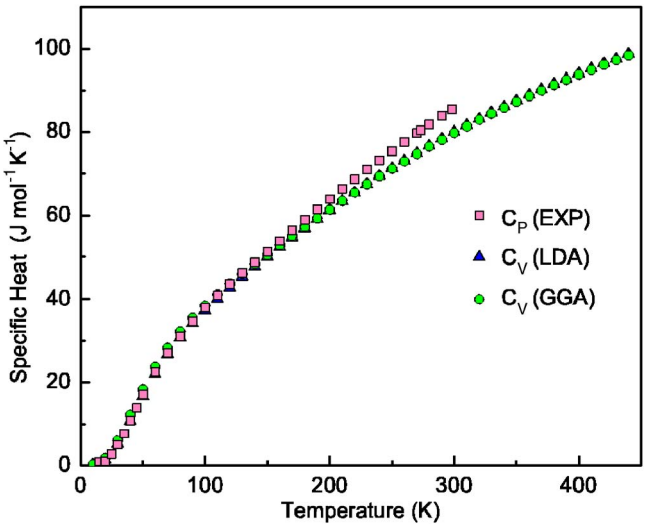

FIG. 5. (Color online) Constant-volume specific heat calculated at the experimental lattice parameters using either LDA and GGA together with experimental data up to 300 K (Ref. 12).

$$C_V = \sum_{\mathbf{k},n} \hbar\,\omega_n(\mathbf{k}) \frac{\partial}{\partial T}\left[e^{\frac{\hbar\omega_n(\mathbf{k})}{k_B T}} - 1\right]^{-1} \tag{5}$$

where $[e^{\hbar\omega_n(\mathbf{k})/k_B T}-1]^{-1}$ is the mean number of phonons with energy $\hbar\omega_n(\mathbf{k})$ excited at the given temperature. Figure 5 shows the constant-volume specific heat C_V calculated using Eq. (5) at the experimental volume and compared to the experimentally available data for the constant-pressure specific heat C_P.[12] The agreement between both LDA and GGA calculations and experimental data is very good. Below 170 K GGA results are slightly higher than LDA results and both exhibit the expected T^3 power-law behavior in the low-temperature limit. At high temperatures LDA and GGA give almost identical C_V. The high temperature C_V does not reach a classical limit of 149.6 J/mol K up to 450 K which is just below the melting point of $NaAlH_4$, indicating that not all harmonic vibrations are thermally excited up to the melting point. The discrepancies between the calculated harmonic specific heat C_V and the experimental specific heat C_P above ~170 K are indicative of vibrational anharmonicity. The anharmonicity that results in thermal expansion can be taken into account within a so-called quasiharmonic approximation, where the variation of phonon frequencies with the lattice parameters is considered. As a tetragonal lattice can undergo a nonuniform expansion, i.e., changes in both size and shape, the Helmholtz free energy thus depends on the lattice parameters a and c as follows:

$$F(T,a,c) = E(a,c) + \frac{1}{2}\sum_{\mathbf{k},n} \hbar\,\omega_n(\mathbf{k},a,c) + k_B T \sum_{\mathbf{k},n} \ln\left[1 - e^{-\frac{\hbar\omega_n(\mathbf{k},a,c)}{k_B T}}\right]. \tag{6}$$

Here $E(a,c)$ represents a static lattice energy calculated with LDA or GGA, while the sum of the other two terms that depend on vibrational frequencies $\omega_n(\mathbf{k},a,c)$ represents the vibrational contribution to the free energy for a given lattice parameters a and c. In this approach further anharmonic terms due to the phonon-phonon interactions which result in explicit temperature dependence of phonon frequencies are ignored. The LDA and GGA harmonic phonon frequencies are calculated at six different sets of lattice parameters a and c and interpolated for points inbetween. At each temperature the vibrational part of the free energy has a nearly linear dependence on the lattice parameters. Linear and bilinear fit were equally good and we used a bilinear form to interpolate the vibrational part of the free energy on a grid of points between calculated points. The total energies of the static lattice for the same grid of (a,c) points are also calculated. The equilibrium lattice parameters at each temperature are determined by minimizing the free energy in Eq. (6). The LDA and GGA lattice parameters with respect to their static lattice values were plotted in Fig. 6 as a function of temperature. Both approximations show that the lattice expands on heating. At zero temperature the data in Fig. 6 correspond to the changes of lattice parameters due to zero-point vibrations. The modified lattice parameters are also listed in Table I. The expansion along the c direction is much more pronounced in the GGA calculation at zero temperature. Furthermore GGA predicts a larger expansion of lattice parameters than LDA at all temperatures. The expansion is anisotropic and the lattice constant c expands much more than constant a. The anisotropic expansion has been observed on heating from room temperature up to ~423 K where an expansion of 0.2% along a and 1% along c were reported.[6] Our LDA calculations predict 0.4% and 1.1% expansion in a and c, respectively, while GGA predicts a 0.6% expansion in a and 1.4% expansion in c. Also, the expansion mainly along the c axis was observed on heating from 10 K up to room temperature,[9] the data indicating that a expands 0.6% and c expands 1.4%. This can be compared to calculated predictions of a and c expanding 0.5 and 1.2%, respectively, within LDA and 0.7 and 1.7%, respectively, within GGA. Such an anisotropic expansion can be explained if we

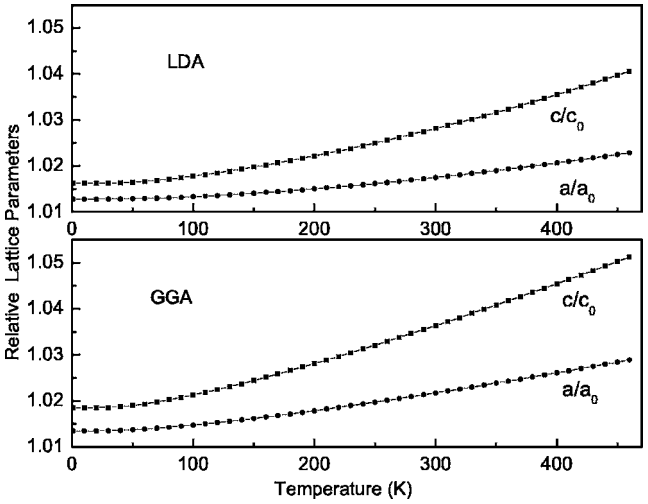

FIG. 6. Temperature dependence of the change of relative lattice parameters with respect to lattice parameters of static lattice (T=0, no zero-point motion) for both LDA and GGA.

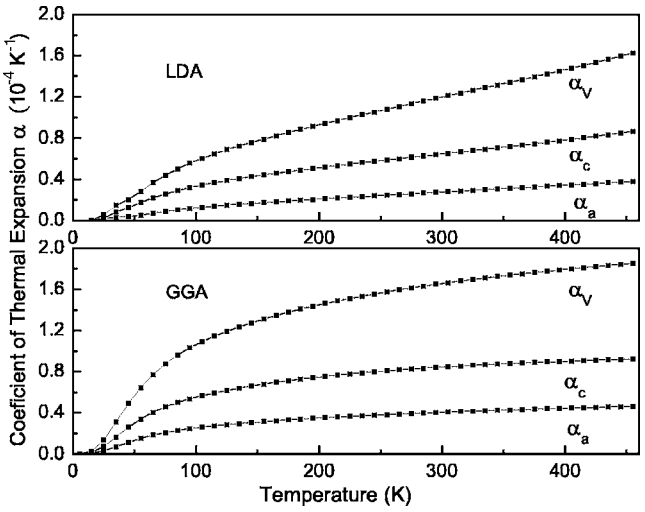

FIG. 7. Calculated thermal expansion coefficients using LDA and GGA. α_a and α_c are expansion coefficients along a and c crystal axes and α_V is the volume expansion coefficient.

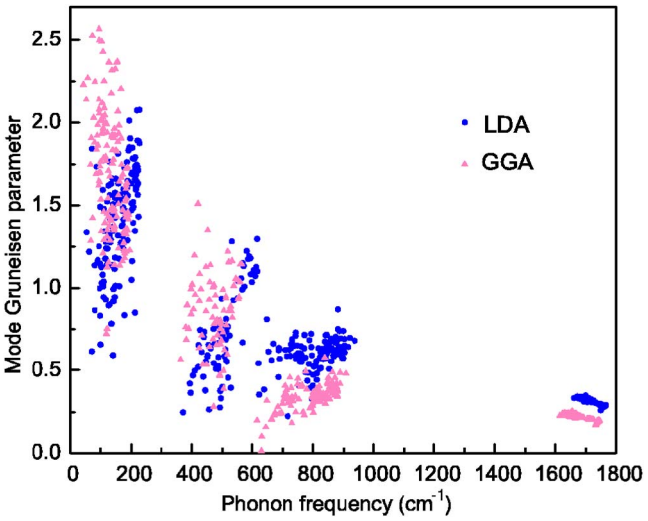

FIG. 8. (Color online) Mode Grüneisen parameters as a function of frequency for phonons on a $4\times4\times4$ grid in the first Brillouin zone. Both LDA and GGA results are shown.

consider the interaction between Na^+ and AlH_4^-. The nearest neighbor distance between Na^+ and AlH_4^- in the vertical direction (c) and along the basal plane would be equal if the c/a ratio equals 2, and in this case, one would expect a uniform binding strength in all directions and an isotropic thermal expansion of the lattice. However the c/a ratio in $NaAlH_4$ is bigger than 2 at all temperatures and the interion interaction along the c direction is less strong than within the basal plane, resulting in an anisotropic expansion with the c lattice constant expanding more than a. The c/a ratios of LDA and GGA static equilibrium structures are 2.19 and 2.22, respectively. This seems to be consistent with the fact that GGA gives a larger thermal expansion along c direction in Fig. 6. The thermal expansion coefficient governing the expansion in a and c directions are diagonal components of the thermal expansion tensor and were obtained as follows:

$$\alpha_{a_i} = \frac{1}{a_i}\frac{da_i}{dT}, \tag{7}$$

where a_i stands for a and c. The volume expansion coefficient α_V is given as trace of the expansion tensor, namely $\alpha_V = 2\alpha_a + \alpha_c$. The coefficients of thermal expansion are plotted in Fig. 7 for both LDA and GGA. In comparison with available theoretical results, our temperature changes of lattice parameters in the LDA approximation agree well with the LDA calculation in Ref. 8. The equilibrium volumes at different temperatures reported in the GGA-PAW calculation[17] agree reasonably well with our GGA calculations. However, the thermal expansion coefficients of the same study show a linear dependence with temperature and overall do not agree with our predictions within the GGA or LDA approach. This discrepancy is most likely due to the possibility of anisotropic expansion in tetragonal structures and the necessity to parametrize free energy and vibrational frequencies with respect to both lattice parameters a and c, instead of the volume only when free energy minimization is performed. Our results show such anisotropy in the lattice expansion that was also observed in the experiment. To understand the behavior of the volume thermal expansion coefficient, we can examine the frequency dependence of the mode Grüneisen parameter defined for each normal mode as follows:

$$\gamma_{n,\mathbf{k}} = -\frac{\partial \ln \omega_n(\mathbf{k})}{\partial \ln V}. \tag{8}$$

Figure 8 shows the mode Grüneisen parameters for a $4\times4\times4$ grid of k points in the Brillouin zone estimated at the LDA and GGA equilibrium volume, respectively, and keeping the c/a ratio fixed. $\gamma_{n,\mathbf{k}}$ measures the extent of anharmonicity through the relative change of normal mode frequencies with respect to a relative change in volume. Figure 8 shows the largest such changes for the low frequency translatory modes and $\gamma_{n,\mathbf{k}}$ decreases with increasing frequencies. The high frequency hydrogen stretching modes show a very small mode Grüneisen parameter. The anharmonicity in thermal expansion is dominated by the low-energy vibrations in $NaAlH_4$. GGA calculated $\gamma_{n,\mathbf{k}}$ are higher at the low frequencies than LDA, while in the two highest frequency bands GGA estimates of $\gamma_{n,\mathbf{k}}$ are well below those of LDA. Our LDA values of the mode Grüneisen parameters at the Γ point for the Raman active modes agree well with those reported in Ref. 8. The current more extensive results over the whole spectrum allow us to assess the anharmonicity of all phonon modes and to draw conclusions on the modes making major contributions to the thermal expansion.

The knowledge of the volume expansion coefficients can be used to find an approximate estimate of the specific heat at constant pressure, C_P, as follows:

$$C_P = C_V + \alpha(T)^2 V(T) T B(0), \tag{9}$$

where B was assumed not to change significantly with temperature and the constant value at $T=0$ was used. Figure 9 shows the temperature dependence of C_P for both LDA and GGA results at the experimental volume together with mea-

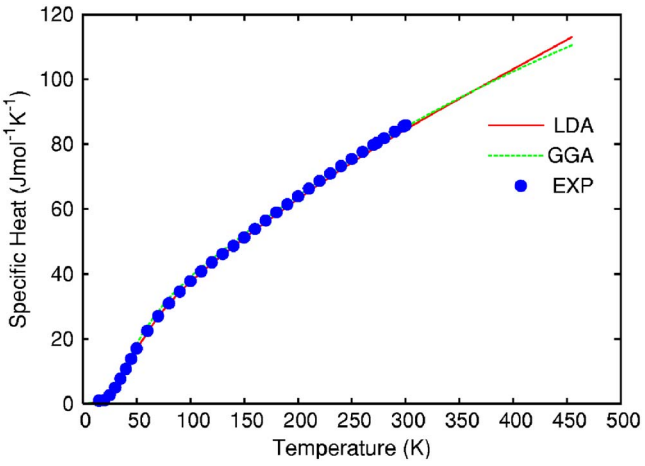

FIG. 9. (Color online) The specific heat at constant pressure for LDA and GGA and experimental results up to 300 K.

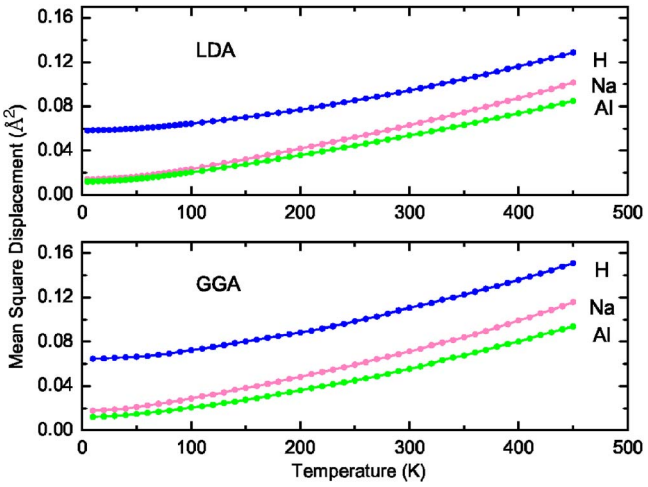

FIG. 10. (Color online) Temperature dependence of the mean square displacements of atoms about their equilibrium positions calculated using LDA and GGA.

sured data up to 300 K. The agreement between calculated and measured values is very good and indicates that up to 300 K the anharmonicity in $NaAlH_4$ can be described by the quasiharmonic approximation. Our results for both C_V (Fig. 5) and C_P (Fig. 9) agree better with experimental values than those reported in Ref. 17, probably due to the fact that our calculation was performed at the experimental volume. At higher temperatures especially closer to the melting point, the crystal is expected to become more anharmonic and the quasiharmonic approach may not be sufficient to describe all anharmonic effects.

The localization of the ionic species around their thermal equilibrium positions can be probed by calculating their mean square displacements. In order to calculate the temperature dependent amplitudes of the mean square displacements of atoms in the vibrating lattice, we use the following expression:

$$\langle \mathbf{u}_n^2 \rangle = \int_0^{\omega_{max}} \frac{3N\hbar}{2m_n\omega} \coth\left(\frac{\hbar\omega}{2k_BT}\right) g_n(\omega) d\omega. \qquad (10)$$

Here n denotes an atom and $g_n(\omega)$ is a projected density of states for atom n. At the equilibrium lattice parameters at each temperature mean square displacements are estimated. Thus, the anharmonic effects due to thermal expansion within the quasiharmonic approximation were included. The LDA and GGA results are shown in Fig. 10. The GGA approach predicts somewhat larger deviations from the equilibrium positions than LDA. The displacements of all atoms show nonlinear variations with temperature especially as temperature increases toward the melting temperature. The experimental melting temperature is ~458 K. Furthermore, we can use the empirical Lindemann melting criterion[32] to estimate the melting point. This criterion suggests that solids melt at temperature T_m for which root mean square displacement $\langle \mathbf{u}_n^2 \rangle^{1/2}$ exceeds a certain fraction of the nearest neighbor distance l. Typical values of the ratio $\xi = \langle \mathbf{u}_n^2 \rangle^{1/2}/l$ are of the order of magnitude 0.1 for most of the elemental structures. Using the thermal displacements of sodium we can estimate a melting temperature of $NaAlH_4$ to be 460 K for both LDA and GGA. This estimate is very close to the experimentally measured T_m. As the thermal displacement is related to the Debay-Waller factor we can compare our calculated displacements with reported thermal factors B in the scattering experiments. Our calculated values represent the average for three directional mean square displacements and they are 1.45 for Al, 1.65 for Na, and 2.52 for H at room temperature and 0.32 for Al, 0.37 for Na, and 1.55 for H at 8 K within LDA. The GGA values for B factors are 1.42 for Al, 1.88 for Na, and 2.87 for H at room temperature and 0.32 for Al, 0.45 for Na, and 1.68 for H at 8 K. The temperature B factors at room temperature from the experiments are 1.65 for Al, 2.07 for Na, and 2.623 for H in Ref. 33. Another experiment[27] gave 1.08 for Al, 1.52 for Na, and 2.45 for H(D) at room temperature and 0.45 for Al, 0.29 for Na, and 1.21 for H(D) at 8 K. The reasonable agreement between calculated and measured B factors is evident. Significant mobility of ions at higher temperatures is suggested by the increase in the mean square displacements and agrees with the observation of the time variation in diffraction peak intensities at 150 °C in the *in situ* diffraction experiment.[6] The migration of the Na^+ and AlH_4^- are also possible close to the melting point.

IV. CONCLUSIONS

In summary, we have performed detailed studies of the Lattice dynamics and thermodynamic properties of $NaAlH_4$ within the density functional theory and pseudopotential methods. The optimal ground-state structure is investigated within the LDA and GGA approaches. The zero-point motion has a considerable effect on the calculated lattice parameters, giving rise to a volume expansion of ~4.4% for both LDA and GGA. LDA predicts smaller lattice constants compared with the experiment, both with and without the zero-point motion included. Without the zero-point motion, GGA also underestimates the lattice parameters, while including the zero-point motion the lattice parameters are overestimated.

The bulk moduli estimated within LDA and GGA differ significantly; the GGA value is about 2/3 of the LDA value. This suggests that not only the elastic but also the dynamical properties of $NaAlH_4$ are sensitive to the way the exchange and correlation effects are approximated.

Born effective charges and dielectric permitivities are calculated within the linear response approach. In contrast, the choice of the exchange-correlation functional does not have noticeable effects on these quantities. $NaAlH_4$ exhibits complex vibrational properties at the Γ point. The normal mode is characterized with appropriate assignments within a point group of crystal (4/m). These are related to the mode characters of the T_d point group of individual AlH_4^- that was often used to characterize vibrations within a complex. The Coulomb forces between ions cause a LO-TO splitting for A_u and E_u modes, which were calculated using the Born effective charge and dielectric tensors. The four groups of normal modes can be identified. These are low-frequency translatory modes, librational modes, hydrogen bending modes, and hydrogen stretching modes. At the experimental volume, we find that LDA tends to give larger estimates for normal mode frequencies at the low energies and lower ones for higher energy modes than GGA. The calculated frequencies are in reasonable agreement with the experiment. The phonon dispersion and phonon density of state also show four separated groups of normal modes. The projected phonon density of states indicates that Na and Al atoms are predominantly involved in the low-energy oscillations, while hydrogen motion dominates the three high-energy groups of modes.

A number of thermodynamical properties have been calculated. The specific heats C_V calculated at the experimental volume within the harmonic approximation for both LDA and GGA show very good agreement with experimental data at lower temperatures. The quasiharmonic approach was used to estimate the changes of lattice parameters with temperature. The results indicate an expanding lattice on heating. The expansion is anisotropic and the crystal expands more along the axis c than in the perpendicular direction along axis a. The extent of expansion seems to be correlated with the amount of deviation of the c/a ratio from the ideal value of two.

GGA is found to predict much larger thermal expansion coefficients than LDA, especially in the intermediate range of temperatures between 50 K and the melting point. The mode Grüneisen parameters, an anharmonicity coefficient for individual normal modes, are evaluated at a grid of **k** points in the Brillouin zone. The largest anharmonicity was detected among the low-energy vibrations, while very small values are found for the highest frequency modes. The GGA Grüneisen parameters seem to be larger than those predicted by LDA for the lowest-frequency group of normal modes, while they are evidently smaller than LDA values for modes above 600 cm^{-1}. The anharmonic correction to the constant volume specific heat due to thermal expansion was also calculated. The resulting C_P values for $NaAlH_4$ up to 300 K compare well with the experiment.

The "mobility" of the species in $NaAlH_4$ has been studied through the temperature dependence of the atomic mean-square displacements in the $NaAlH_4$ about their equilibrium position. A good agreement of Deby-Waller factors with scattering experiments is found. The Lindemann empirical criterion is used to predict a melting temperature which agrees very well with the observed value. Even at a temperature close to the melting temperature, the thermal energy ($k_B T_m$) is only sufficient to excite low-energy vibrations involving the translational motion between Na^+ and the AlH_4^- complex. These vibrations are found to be most anharmonic among all normal modes. This suggests that the melting of $NaAlH_4$ involves the breakup of lattice periodicity by large displacements of Na^+ and AlH_4^-, while Al remains in a tetrahedral coordination with hydrogen and the Al-H bond is not broken. It is noted that hydrogen release in pure $NaAlH_4$ does not take place until the temperature is above the melting point.

This work is supported by the Department of Energy under Grants Nos. DE-FG02-97ER45632 and DE-FG02-05ER46229. A research grant from General Electric Global Research is gratefully acknowledged. The computation used resources of the National Energy Research Scientific Computing Center (NERSC), which is supported by the U.S. Department of Energy (Grant No. DE-AC03-76SF00098), and also the resources at the Oak Ridge National Laboratory.

[1] A. Züttel, Mater. Today **9**, 24 (2003).
[2] L. Schlapbach and A. Zuttel, Nature (London) **414**, 353 (2001).
[3] C. M. Jensen and K. J. Gross, Appl. Phys. A **72**, 213 (2001).
[4] B. Bogdanović and M. Schwickardi, J. Alloys Compd. **253-254**, 1 (1997).
[5] O. M. Løvvik, O. Swang, and S. M. Opalka, J. Mater. Res. (to be published), and references therein.
[6] K. J. Gross, S. Gurthie, S. Takara, and G. Thomas, J. Alloys Compd. **297**, 270 (2000).
[7] D. J. Ross, M. D. Halls, A. G. Nazri, and R. F. Aroca, Chem. Phys. Lett. **388**, 430 (2004).
[8] E. H. Majzoub, K. F. McCarty, and V. Ozoliņš, Phys. Rev. B **71**, 024118 (2005).
[9] S. Gomes, G. Renaudin, K. Hagemann, M. P. Sulic, C. M. Jensen, J. Alloys Compd. **390**, 305 (2005).
[10] F. P. Temme and T. C. Waddington, J. Chem. Soc., Faraday Trans. 1 **69**, 783 (1973).
[11] J. Iniguez, T. Yildirim, T. J. Udovic, M. Sulic, and C. M. Jensen, Phys. Rev. B **70**, 060101(R) (2004).
[12] B. Bonnetot, G. Chanine, P. Cloudy, M. Diot, and J. M. Letoffe, J. Chem. Thermodyn. **12**, 249 (1980).
[13] P. Vajeetson, P. Ravindran, R. Vidya, H. Fjellvag, and A. Kjekshus, Appl. Phys. Lett. **82**, 2257 (2003).
[14] S. M. Opalka and D. L. Anton, J. Alloys Compd. **356-357**, 486 (2003).
[15] A. Aguayo and D. J. Singh, Phys. Rev. B **69**, 155103 (2004).

[16] A. Peles, J. A. Alford, Z. Ma, L. Yang, and M. Y. Chou, Phys. Rev. B **70**, 165105 (2004).
[17] X. Ke and I. Tanaka, Phys. Rev. B **71**, 024117 (2005).
[18] P. Hohenberg and W. Kohn, Phys. Rev. **136**, B864 (1964).
[19] W. Kohn and L. Sham, Phys. Rev. **140**, A1133 (1965).
[20] N. Troullier and J. L. Martins, Phys. Rev. B **43**, 1993 (1991).
[21] D. M. Ceperley and B. J. Alder, Phys. Rev. Lett. **45**, 566 (1980).
[22] J. P. Perdew, K. Burke, and M. Ernzerhof, Phys. Rev. Lett. **77**, 3865 (1996).
[23] S. G. Louie, S. Froyen, and M. L. Cohen, Phys. Rev. B **26**, 1738 (1982).
[24] X. Gonze *et al.*, Comput. Mater. Sci. **25**, 478 (2002).
[25] K. V. Belskii, B. M. Bulychev, and A. V. Golubeva, Prog. Inorg. Chem. **28**, 1528 (1983).
[26] J. W. Lauher, D. Dougherity, and P. J. Herley, Acta Crystallogr., Sect. B: Struct. Crystallogr. Cryst. Chem. **35**, 1454 (1979).
[27] B. C. Hauback, H. W. Brinks, C. M. Jensen, K. Murphy, and A. J. Maeland, J. Alloys Compd. **358**, 142 (2003).
[28] M. Born and K. Huang, *Dynamical Theory of Crystal Lattices*, (Oxford University Press, Oxford, 1954).
[29] A. E. Shirk and D. F. Shriver, J. Am. Chem. Soc. **95**, 5904 (1973).
[30] P. Pullumbi, Y. Bouteiller, and L. Manceron, J. Chem. Phys. **101**, 3610 (1994).
[31] G. Herzberg, *Molecular Spectra and Molecular Structure* (Van Nostrand, New York, 1945), Vol. 2, p. 100.
[32] F. Lindemann, Z. Tech. Phys. (Leipzig) **11**, 609 (1910).
[33] V. Ozoliņš, E. H. Majzoub, and T. J. Udovic, J. Alloys Compd. **375**, 1 (2004).